NMR Study of Methane + Ethane Structure I Hydrate Decomposition

Steven F. Dec,* Kristen E. Bowler, Laura L. Stadterman, Carolyn A. Koh, and E. Dendy Sloan, Jr.

Center for Hydrate Research, Department of Chemical Engineering, Colorado School of Mines, Golden, Colorado 80401

Received: January 18, 2007; In Final Form: March 12, 2007

The thermally activated decomposition of methane + ethane structure I hydrate was studied with use of ^{13}C magic-angle spinning (MAS) NMR as a function of composition and temperature. The observed higher decomposition rate of large sI cages initially filled with ethane gas can be described in terms of a model where a distribution of sI unit cells exists such that a particular unit cell contains zero, one, or two methane molecules in the unit cell; this distribution of unit cells is combined to form the observed equilibrium composition. In this model, unit cells with zero methane molecules are the least stable and decompose more rapidly than those populated with one or two methane molecules leading to the observed overall faster decomposition rate of the large cages containing ethane molecules.

Introduction

Natural gas clathrate hydrates (gas hydrates) are materials that form at low temperatures and high pressures.[1] The host lattice consists of water molecules that hydrogen bond to each other to form a variety of cages that trap different sized molecules, such as methane, ethane, and carbon dioxide. Naturally occurring gas hydrates are abundant in permafrost and marine environments[2] and represent a potential energy resource as well as a possible environmental hazard. These compounds also form in gas and oil pipelines disrupting production and in worst case scenarios can cause costly equipment damage and loss of life.[1]

Methane and ethane gas mixtures form the two common gas hydrate structures, Structure I (sI) and Structure II (sII); the structure that forms depends on the gas-phase composition, temperature, and pressure[3] as indicated by the phase diagram shown in Figure 1a. The water lattice cages from which the cubic unit cells of sI and sII are formed are depicted in Figure 1b. Van der Waals and Platteeuw[4] developed a statistical mechanics model to calculate the chemical potential of water in gas hydrates. The chemical potential difference of water in a methane (C1) + ethane (C2) gas hydrate and water in ice, $\Delta\mu_w(h)$, for sI and sII hydrates, respectively, is given by[3]

$$\Delta\mu_w(h) = \Delta\mu_w(h^o) + \frac{RT}{23}[3\ln(1-\theta_{l,C2}-\theta_{l,C1}) + \ln(1-\theta_{s,C1})] \quad (1)$$

$$\Delta\mu_w(h) = \Delta\mu_w(h^o) + \frac{RT}{17}[\ln(1-\theta_{l,C2}-\theta_{l,C1}) + 2\ln(1-\theta_{s,C1})] \quad (2)$$

The various terms in eqs 1 and 2 are defined as follows: $\Delta\mu_w(h^o)$ is the chemical potential difference of water in the hypothetical empty hydrate lattice and water in the ice phase, R is the gas constant, T is the absolute temperature, $\theta_{l,C2}$ is the fractional occupancy of ethane in the large cage of sI or sII ($5^{12}6^2$ or $5^{12}6^4$, respectively), $\theta_{l,C1}$ is the fractional occupancy of methane in the large cage of sI or sII, and $\theta_{s,C1}$ is the fractional occupancy of methane in the small cage (5^{12}) of sI or sII. It is clear from inspection of eqs 1 and 2 that as the fractional occupancy of the cages increases the hydrate becomes more stable because the chemical potential of water is lowered.

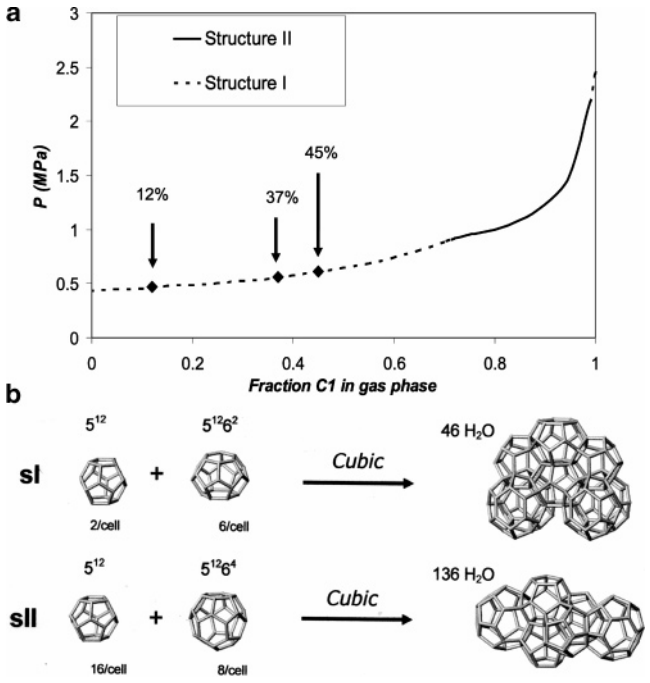

Figure 1. (a) Pressure versus methane gas-phase composition for the methane + ethane + water system at 272 K. Arrows indicate methane gas-phase compositions used in this work. (b) Polyhedral cages and partial unit cells of sI and sII clathrate hydrates.

The thermodynamics of gas hydrates are fairly well established[1] but studies of kinetic processes, especially at the microscopic level, are more limited. NMR and Raman spectroscopy and X-ray and neutron diffraction have been employed to follow the course of hydrate formation and dissociation in some cases.

The X-ray and neutron diffraction studies reported to date have mostly focused on overall gas hydrate formation rates and

10.1021/jp070442y CCC: $37.00
Published on Web 04/26/2007

the structural changes of water in the hydration sphere of the gas. Time-resolved X-ray diffraction has been used to follow the formation process of dissolved gas in aqueous solution to gas hydrate.[5] A number of studies have employed time-resolved neutron diffraction techniques to measure the overall kinetics of hydrate formation[6−9] as well as to study the structural changes occurring in the water solvation shell of the gas guest.[10,11]

An early NMR study used hyperpolarized ^{129}Xe NMR to monitor the formation of xenon sI hydrate from xenon gas and H_2O(s), using time-resolved NMR.[12] A subsequent and more comprehensive hyperpolarized ^{129}Xe NMR study[13] also followed the decomposition of xenon sI hydrate when the material was exposed to vacuum. In both studies, the rate at which xenon occupied the small sI cage occurred more rapidly than the rate at which xenon occupied the large cage of sI during formation of the hydrate despite the fact that there are three times more large cages than small cages in sI hydrate. In contrast, the xenon sI hydrate decomposition showed no preferential rate of dissociation of either cage.[13] Raman spectroscopy was used to monitor the formation of methane sI hydrate from methane gas and H_2O(l).[14] The occupation of the small cage by methane was found to occur at a higher rate than that observed for methane gas occupying the large cage. NMR was also used to measure kinetic parameters for the formation of sII hydrate from mixtures of methane and propane gas and H_2O(s).[15] In this case, the large cage of sII was found to be occupied by propane at a faster rate than methane occupied the small cage even though there are two times more small cages in the sII hydrate. While no complete theoretical explanation for the hypothesis has been presented to date, it has been suggested that the cage that is observed to form more rapidly in these three NMR studies is based on the gas size to cage size ratio, that is, the closer this ratio is to unity the more stable the cage.[1]

A more recent study has used time-resolved ^{13}C magic-angle spinning (MAS) NMR to study the decomposition of methane sI hydrate.[16] In contrast to the formation studies described above, both the large and small cages occupied by methane gas were found to decompose at the same rate. Both the methane and xenon sI hydrate decomposition studies suggest that sI hydrate unit cells of these gas hydrates decompose as a single entity, at least on the time scale of the NMR measurements.

The focus of the present work is to further probe the mechanism of gas hydrate decomposition. Gas hydrates formed from mixtures of methane and ethane gases provide the ability to vary the composition of the gases in the hydrate phase as well as the structure of the hydrate phase. In this way, the decomposition of methane and ethane gas hydrates can be studied as a function of stability (which depends on the composition of the hydrate) of the gas hydrate, as described by eqs 1 and 2.

Experimental Section

Sample Preparation. The equipment and procedures used to prepare gas hydrates in sealed glass ampoules have been described elsewhere.[16] In this work enriched $^{13}CH_4$ (99%, Cambridge Isotope Laboratory) and enriched $^{13}CH_3CH_3$ (99%, Isotec) were used to form methane + ethane hydrates with various compositions. For example, to prepare a sample consisting of approximately 50% methane hydrate, about equal volumes of methane and ethane were condensed into the high-pressure glass cell containing about 50 mg of powdered H_2O(s). The initial pressures of the sealed samples were on the order of 1−3 MPa. Note that all methane + ethane gas mixtures initially formed a mixture of sI and sII hydrate. To obtain pure sI (or sII) hydrate only, samples containing the sI + sII mixture were decomposed and sI (or sII) hydrate was subsequently allowed to reform from the resulting methane + ethane gas mixture and H_2O(l). The pure hydrate phase produced in this manner was a function of the resulting methane + ethane gas-phase composition. The gas-phase composition actually produced was determined with ^{13}C MAS NMR spectroscopy. Each synthesis took on the order of 1 to 3 months. The equilibrium gas-phase compositions are indicated in Figure 1a.

NMR Spectroscopy. All ^{13}C MAS NMR spectra were recorded on a Chemagnetics Infinity 400 NMR spectrometer operating at 100.6 MHz for ^{13}C. Proton decoupling fields of 50 kHz and MAS speeds of about 2 kHz were used. Two different types of ^{13}C MAS NMR spectra were obtained. Standard single-pulse excitation (90° pulses of 5 μs) and various pulse delays, depending on the spin−lattice time (T_1), were used to record fully relaxed, high signal-to-noise ratio spectra at various temperatures. Time-resolved ^{13}C MAS NMR spectra were recorded with single-pulse excitation (45° pulses of 2.5 μs) and various pulse delays in the hydrate dissociation experiment. Under the conditions of the time-resolved ^{13}C MAS NMR experiment with a pulse repetition rate of T_R the magnetization $M(T_R)$ is given by[17]

$$M(T_R) = M_{eq}\frac{1 - e^{(-T_R/T_1)}}{1 - \cos(45^o)e^{(-T_R/T_1)}} \qquad (3)$$

M_{eq} is the equilibrium magnetization. $M(T_R)$ reached its steady state value after about five pulse repetitions. Spin−lattice relaxation times were measured by using a standard inversion−recovery pulse sequence.[18]

The methylene carbon resonance line of adamantane was used as an external chemical shift standard (via sample substitution) and was assigned a value of 38.83 ppm.[16] The spectrometer was equipped with Chemagnetics solid-state MAS speed and temperature controllers.

Temperature calibration at the position of the sample has been described.[16] Thermal activation of the samples was achieved with a temperature-jump method by increasing the set temperature of the temperature controller. The sample reached the final temperature of the temperature-jump, T_J, in about 80 s. Temperature gradients across the sample are negligible due to the small sample size (∼50 mg). Details regarding each thermally activated decomposition experiment are provided in the figure captions.

Results and Discussion

Figure 2 shows typical ^{13}C MAS NMR spectra of C1−C2 sI hydrate, initially at equilibrium (bottom of figure) and after partial decomposition (top of figure). Five different ^{13}C isotropic resonance lines appear in each spectrum. The hydrate phase ^{13}C resonance lines are due to C2 in the large cage of sI hydrate at 7.8 ppm, C1 in the small cage of sI hydrate at −3.8 ppm, and C1 in the large cage of sI hydrate at −6.0 ppm.[3] The ^{13}C resonance line at about −10.6 ppm is due to gas-phase C1.[19] By process of elimination the ^{13}C resonance line at about 3.6 ppm is due to gas-phase C2. The effect of raising the temperature of the sample yields the expected result: the relative intensities of C1 and C2 in the hydrate phase decrease while the relative intensities of C1 and C2 in the gas phase increase in this closed system.

Figure 3 shows one in a series of time-resolved ^{13}C MAS NMR spectra of a C1−C2 gas hydrate sample where the decomposition process was thermally activated by increasing

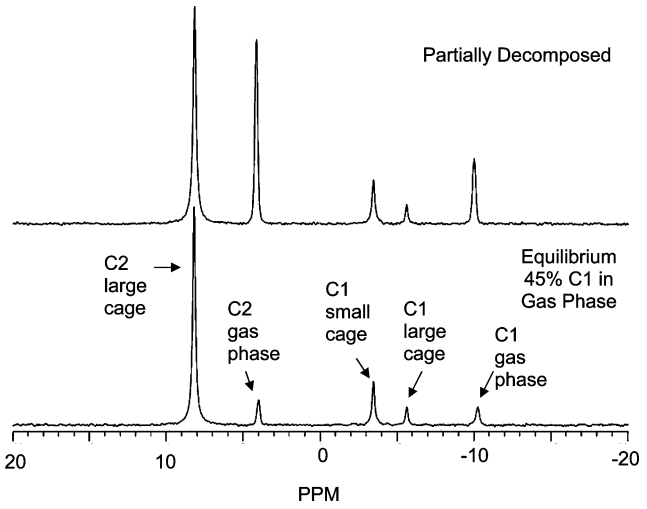

Figure 2. ^{13}C MAS NMR spectra (100.6 MHz) of a C1−C2 sI hydrate at equilibrium and partially decomposed. The sample was initially equilibrated at 272 K to form sI hydrate. The NMR spectrum was recorded at 273 K.

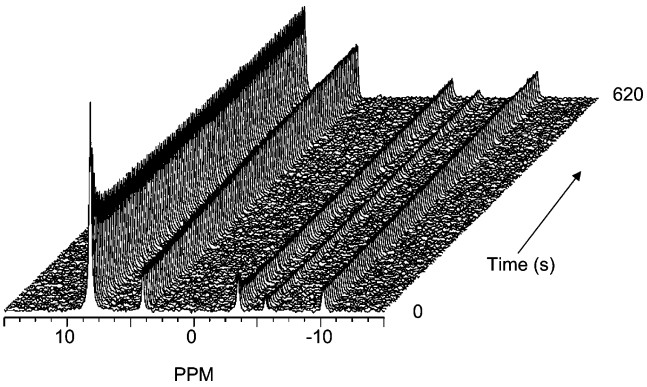

Figure 3. Time-resolved ^{13}C MAS NMR spectra (100.6 MHz) of C1−C2 sI hydrate with an initial C1 gas-phase composition of 45% with a temperature-jump from an initial temperature of 279 K to $T_J = 281$ K. The acquisition time was 0.1024 s and $T_R = 3.1024$ s.

the temperature of the sample at time $t = 0$. The observed ^{13}C MAS NMR spectra are typical for this type of thermally activated decomposition process. During the course of the first five pulse repetitions, the intensity of all peaks is observed to decrease because each resonance is partially saturated by the rapid pulse repetition rate; this is most readily seen for the C2 hydrate phase peak in this case. After the first few pulses, the intensities of each of the ^{13}C resonance lines change as a function of time, indicating that the C1−C2 sI hydrate and C1−C2 gas-phase compositions were changing. This is more readily seen in Figure 4 where the integrated relative intensities, I, corrected according to eq 3 with the average T_1 values summarized in Table 1, are plotted for one typical decomposition experiment (average T_1 values were used because the ^{13}C T_1 for the various C1 and C2 sites are a slowly varying function over the temperature range of interest in this work). Figure 4 shows that the relative intensity of the C2 ^{13}C resonance lines in both the hydrate and gas phases show the greatest relative intensity decrease and increase, respectively.

The data of Figure 4 correspond to one of four time-resolved ^{13}C MAS NMR decomposition experiments for this C1−C2 sI hydrate. Each of the four successive decomposition experiments had a higher T_J. All the experiments in this series have the same general appearance as a function of time. Some C1−C2 hydrate decomposes during the first 80 s while the sample approaches

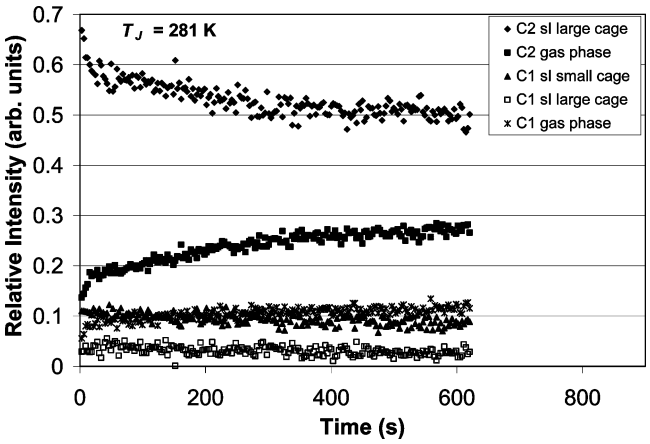

Figure 4. Relative integrated intensities of ^{13}C resonance lines versus time obtained from a thermally activated C1−C2 sI hydrate decomposition experiment for a C1−C2 sI hydrate with an initial C1 gas-phase composition of 45%. The acquisition time was 0.1024 s and $T_R = 3.1024$ s. The temperature-jump was from an initial temperature of 279 K to $T_J = 281$ K.

TABLE 1: Spin−Lattice Relaxation Times of C1−C2 sI Hydrates

site	T (K)	T_1 (s)
initial C1 gas-phase composition = 45%[a]		
C2 sI large cage	258	12.0 ± 0.7
	263	12.2 ± 0.5
	268	11.6 ± 0.5
	273	11.5 ± 0.5
	average	11.8
C2 gas phase	258	0.8 ± 0.2
	263	0.7 ± 0.2
	268	0.6 ± 0.2
	273	0.7 ± 0.2
	average	0.7
C1 sI small cage	258	9.9 ± 0.5
	263	10.2 ± 0.3
	268	9.4 ± 0.5
	273	9.6 ± 0.6
	average	9.8
C1 sI large cage	258	8.8 ±0.8
	263	8.5 ± 0.5
	268	8.7 ± 0.8
	273	8.6 ± 0.5
	average	8.7
C1 gas phase	258	0.17 ± 0.01
	263	0.16 ± 0.01
	268	0.16 ± 0.01
	273	0.17 ± 0.01
	average	0.17
initial C1 gas-phase composition = 37%[a,b]		
C2 sI large cage	268−278	2.2 ± 0.1
C2 gas phase	268−278	0.8 ± 0.2
C1 sI small cage	268−278	1.5 ± 0.1
C1 sI large cage	268−278	1.2 ± 0.1
C1 gas phase	268−278	0.17 ± 0.01
initial C1 gas-phase composition = 12%[a,b]		
C2 sI large cage	253−270	5.9 ± 0.3
C2 gas phase	253−270	0.8 ± 0.2
C1 sI small cage	253−270	4.5 ± 0.2
C1 sI large cage	253−270	∼4.5
C1 gas phase	253−270	0.17 ± 0.01

[a] Initial gas-phase composition corresponds to the equilibrium composition obtained after the hydrate sample was melted and allowed to reform; see Sample Preparation. [b] Average T_1 over temperature range specified.

T_J; this is evident from the decrease in intensity of the ^{13}C NMR resonance lines of C1 and C2 in the hydrate phase as well as an increase of intensity of the ^{13}C NMR resonance lines of C1

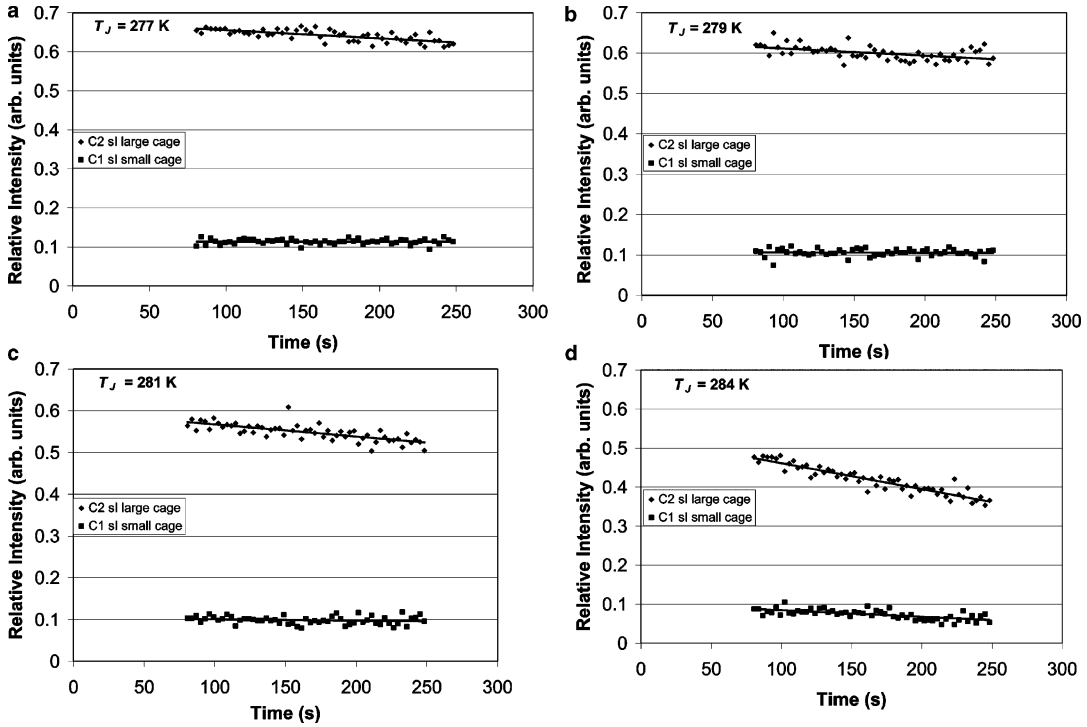

Figure 5. Relative integrated intensities of C2 sI large cage and C1 sI small cage data of a series of experiments similar to Figure 4 for the time period of 80−250 s: (a) temperature-jump from an initial temperature of 275 K to $T_J = 277$ K; (b) temperature-jump from an initial temperature of 277 K to $T_J = 279$ K; (c) temperature-jump from an initial temperature of 279 K to $T_J = 281$ K; and (d) temperature-jump from an initial temperature of 281 K to $T_J = 284$ K.

and C2 in the gas phase. Between about 80 and 250 s the C1−C2 hydrate decomposes at its fastest rate. After approximately 250 s the intensity of all C1 and C2 ^{13}C NMR resonance lines approaches a final value because the C1−C2 sI hydrate decomposition process ceases due to the establishment of a new stable condition at the higher temperature and pressure of the system.

For the purposes of the present work the most interesting time period of each of the C1−C2 sI hydrate decomposition experiments described by the typical data set of Figure 4 is that where the hydrate decomposes at its fastest rate, that is, the time period starting at about 80 s. The relative intensities of the C2 sI large cage and C1 sI small cage are plotted versus time for the time period 80 to 250 s in Figure 5a−d for the set of four successive decomposition experiments. The initial decomposition rate (rate of intensity decrease) as determined from the linear fit of the data in Figure 5a−d are listed in Table 2. It is noted that the decay rate of the C2 sI large cage ^{13}C NMR resonance line is divided by a factor of 3 to normalize the rate data to a per cage basis. It is also noted that the decay rate of the C1 sI small cage intensity for the decomposition experiments with the lowest two temperatures is virtually zero.

The data in Figure 5a−d and Table 2 show that both the C2 sI large cage and C1 sI small cage decomposition rates increase with increasing T_J. It is also evident that the ratio, on a per cage basis, of the C2 sI large cage decomposition rate to the C1 sI small cage decomposition rate is large at low T_J and approaches a value of ∼1 as T_J increases. These results clearly demonstrate that C2 sI large cages decompose more readily than C1 sI small cages.

One possible interpretation of this result is that the C2 large cage moiety of a C1−C2 sI hydrate is less stable than the C1 small cage of a C1−C2 sI hydrate. If this hypothesis is correct it contradicts a commonly held view where more stable structures are formed when the size of the gas molecule more closely matches the size of the confining cage.[1] On this size ratio basis, the C2 sI large cage is more stable than the C1 sI small cage.

TABLE 2: Initial Decomposition Rates of the C1 sI Small Cage and the C2 sI Large Cage of C1−C2 sI Hydrates and the Ratio of the C2 sI Large Cage to the C1 sI Small Cage Decomposition Rates

T_J (K)	$^1/_3(dI_{l,C2}/dt)$ (10^4 cage^{-1} s^{-1})	$dI_{s,C1}/dt$ (10^4 cage^{-1} s^{-1})	$[^1/_3(dI_{l,C2}/dt)]/[dI_{s,C1}/dt]$
initial C1 gas-phase composition = 45%[a]			
277	-0.7 ± 0.3	∼0	≫1
279	-0.6 ± 0.4	∼0	≫1
281	-0.8 ± 0.4	-0.4 ± 0.3	2
284	-2.2 ± 0.3	-1.7 ± 0.3	1.3
initial C1 gas-phase composition = 37%[a]			
269	-6.2 ± 0.8	-3.4 ± 0.9	1.8
initial C1 gas-phase composition = 12%[a]			
279	-2.0 ± 0.9	-0.9 ± 0.8	2.2

[a] Initial gas-phase composition corresponds to the equilibrium composition obtained after the hydrate sample was melted and allowed to reform; see Sample Preparation.

Equation 1 provides the basis for a more plausible explanation of the results of the C1−C2 sI hydrate decomposition experiments summarized in Figure 5a−d and Table 2. At equilibrium the chemical potentials of water in hydrate and water in ice are equal. Hence $\Delta\mu_w(h) = 0$ and eq 1 can be rearranged to yield

$$\Delta\mu_w(h^o) = -\frac{RT}{23}[3\ln(1-\theta_{l,C2}-\theta_{l,C1}) + \ln(1-\theta_{s,C1})] \quad (4)$$

The value of $\Delta\mu_w(h^o)$ has been determined by a number of workers.[20,21] Here $\Delta\mu_w(h^o) = 1263$ J mol^{-1} is used.[21] With the relative intensities of the various C1 and C2 sites measured using ^{13}C MAS NMR listed in Table 3 and eq 4, the fractional occupancies summarized in Table 3 are calculated. The large cage of this C1−C2 sI hydrate is nearly 100% occupied while

TABLE 3: Equilibrium ^{13}C Relative Intensities and sI Hydrate Phase Fractional Occupancies of C1−C2 sI Hydrates

site	rel intensity	fractional occupancy
initial C1 gas-phase composition = 45%[a]		
C2 large cage	0.71	0.93 ± 0.01
C2 gas phase	0.06	
C1 small cage	0.13	0.51 ± 0.02
C1 large cage	0.04	0.06 ± 0.03
C1 gas phase	0.05	
initial C1 gas-phase composition = 37%[a]		
C2 large cage	0.36	0.95 ± 0.01
C2 gas phase	0.37	
C1 small cage	0.05	0.43 ± 0.02
C1 large cage	0.01	0.03 ± 0.03
C1 gas phase	0.21	
initial C1 gas-phase composition = 12%[a]		
C2 large cage	0.71	0.96 ± 0.01
C2 gas phase	0.20	
C1 small cage	0.04	0.16 ± 0.02
C1 large cage	0.01	0.03 ± 0.03
C1 gas phase	0.04	

[a] Initial gas-phase composition corresponds to the equilibrium composition obtained after the hydrate sample was melted and allowed to reform; see Sample Preparation.

SCHEME 1

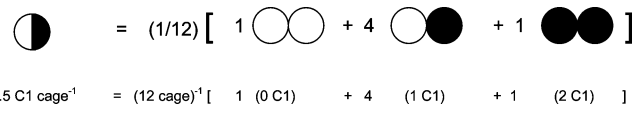

the small cage has a fractional occupancy $\theta_{s,C1} = 0.51 \pm 0.02$. Because there cannot be 0.51 C1 molecule in any one unit cell of a gas hydrate, a distribution of unit cells must exist at equilibrium. Figure 1b indicates that there are two small cages per unit cell in an sI hydrate. One possible distribution of unit cells (of a large number of distributions) that would yield, for example, 0.5 C1 molecule per unit cell corresponds to that shown in Scheme 1. Each pair of open circles represents the two empty small cages of one sI unit cell and each filled circle represents a small cage occupied by one C1 molecule (the structure on the left-hand side of the equality sign in Scheme 1 depicts a hypothetical unit cell containing 0.5 C1 molecule which is, of course, never observed). The right-hand side of Scheme 1 indicates that of the six unit cells, one unit cell contains zero C1 molecules, four unit cells contain one C1 molecule, and one unit cell contains two C1 molecules. Thus, there are six C1 molecules in the twelve small cages of the six unit cells yielding an overall fractional occupancy of 0.5 C1 molecule per cage. During the start of a decomposition experiment the C1−C2 sI hydrate is no longer in equilibrium and eq 1 indicates that those unit cells that contain two C1 molecules will be more stable than those that contain one C1 molecule, which in turn will be more stable than those unit cells that contain zero C1 molecules. The predictions of this model are provided by considering two extreme cases. For the case where only unit cells with zero C1 molecules in the small cages and six C2 molecules in the large cages decompose, the ratio of the decomposition rate of the C2 large cage to that of the C1 small cage is infinitely large. At the other extreme where all small cages are occupied by C1 molecules and all large cages are occupied by C2 molecules, the ratio of the decomposition rate of the C2 large cage to that of the C1 small cage would be one on a per cage basis. Hence, a model that describes the set of decomposition experiments summarized in Figure 5a−d and Table 2 is one where unit cells that contain zero C1 molecules decompose more rapidly than those unit cells that contain one or two C1 molecules in the small cages. This is consistent with the observations where the decomposition rate of the C2 large cage approaches the decomposition rate of the C1 small cage on a per cage basis as more and more hydrate decomposes, that is, as T_J of the set of decomposition experiments increases a larger fraction of the remaining unit cells contain small cages occupied by C1.

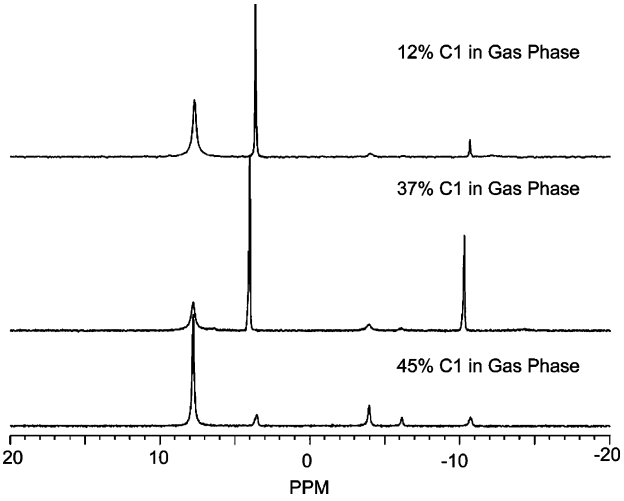

Figure 6. ^{13}C MAS NMR spectra (100.6 MHz) of C1−C2 sI hydrates with different initial compositions. Samples initially equilibrated at 272 K. NMR spectra were recorded at 273, 267, and 275 K for the 45%, 37%, and 12% C1 gas-phase composition samples, respectively.

Additional evidence in support of a unit cell distribution model effect is obtained by considering the results of decomposition experiments for C1−C2 sI hydrates with different initial compositions. The ^{13}C MAS NMR spectra of three different C1−C2 sI hydrates are shown in Figure 6 including the ^{13}C MAS NMR spectrum of the C1−C2 sI hydrate of Figure 2 with its initial composition. Note that the position of the C1 and C2 ^{13}C resonance lines in the gas-phase varies due to different pressures of the three different samples. From the relative intensities of the ^{13}C resonance lines (observed relative intensities corrected to their equilibrium values by using eq 3 and T_1 values provided in Table 1) of Figure 6 and eq 4 the fractional occupancies of C1 and C2 in the large and small cages of each of these C1−C2 sI hydrates can be estimated; these results are summarized in Table 3.

Figure 7a−d shows the relative intensities as a function of time obtained from the time-resolved ^{13}C MAS NMR spectra recorded during the thermally activated decomposition of the 12% and 37% C1 gas-phase samples. Because the C2 sI large cage and C1 sI small cage decomposition rates depend on T_J, the T_J value that yielded the highest decomposition rates was chosen for each sample composition. One such comparison is shown in Figure 8 where the decomposition rate ratio (on a per cage basis) of C2 sI large cage to C1 sI small cage is plotted versus the C1 sI small cage fractional occupancy from Table 3. It is evident that as the C1 sI small cage fractional occupancy decreases the decomposition rate ratio increases. This result is consistent with the unit cell distribution model proposed in this work.

Another model that can be discussed is one where the sI unit cells randomly dissociate and the relative decomposition rate increases as the C1 sI fractional occupancy decreases simply because there are fewer C1 sI small cages available to dissociate. Considering Scheme 1 with all large cages occupied by C2,

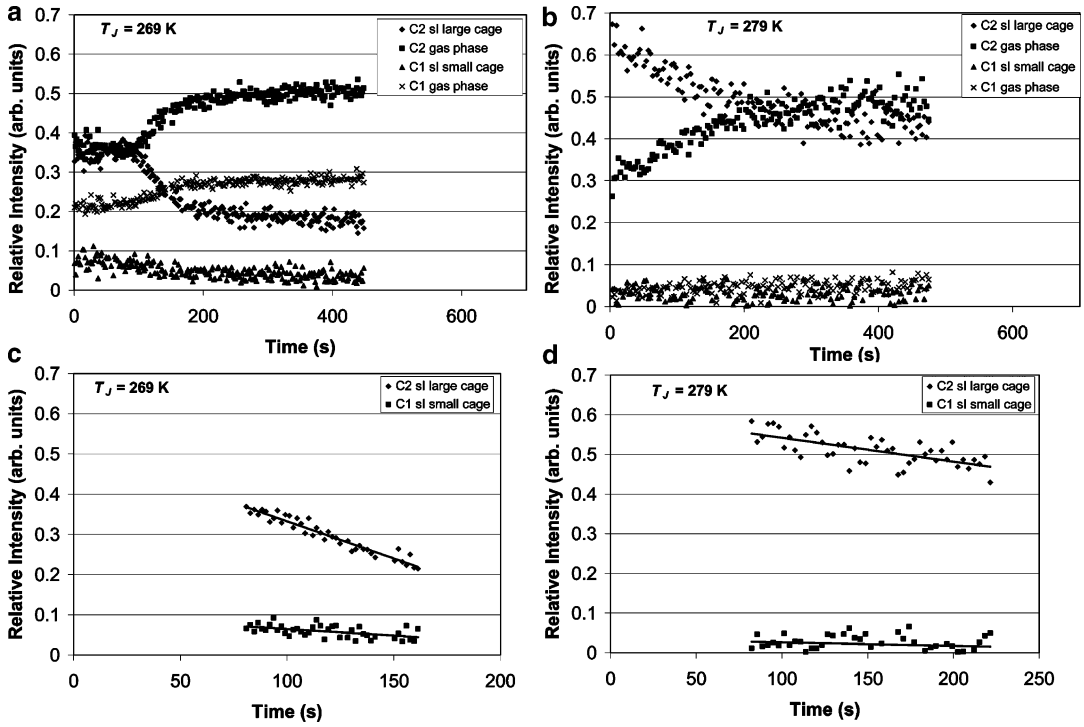

Figure 7. Relative integrated intensities of ^{13}C resonance lines obtained from 37% and 12% C1 gas-phase composition samples shown in Figure 6 versus time: (a) 37% C1 gas-phase composition with a temperature-jump from an initial temperature of 267 K to $T_J = 269$ K (acquisition time was 0.32768 s and $T_R = 1.82768$ s); (b) 12% C1 gas-phase composition with a temperature-jump from an initial temperature of 275 K to $T_J = 279$ K (acquisition time was 0.16384 s and $T_R = 3.16384$ s); (c) C2 sI large cage and C1 sI small cage relative intensities versus time for a time period from about 80 to 250 s for experiment described in part a; and (d) C2 sI large cage and C1 sI small cage relative intensities versus time for a time period from about 80 to 250 s for the experiment described in part b.

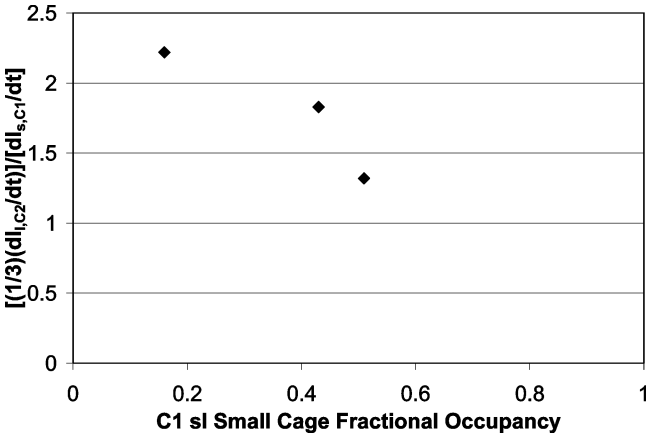

Figure 8. Decomposition rate ratio on a per cage basis of the C2 sI large cage to the C1 sI small cage versus the C1 sI small cage fractional occupancy indicating that C1−C2 sI hydrates with smaller fractional occupancies of C1 in the small cage have a larger decomposition rate ratio. This observation is consistent with the unit cell distribution model developed in this work.

this model predicts that the ratio of the C2 sI large cage decomposition rate to the C1 sI small cage decomposition rate is two and independent of T_J because the decomposition of any unit cell occurs at random. This model is, therefore, inconsistent with the results of the decomposition experiments summarized in Figure 5a−d and Table 2 and is not considered further.

It is interesting that differences in cage decomposition rates were not observed in either the xenon sI hydrate[13] or the methane sI hydrate[16] decomposition studies. This is almost certainly due to the fact that only one pressure-jump and one temperature-jump, respectively, were considered. In addition, observation of a cage-dependent decomposition rate will be more difficult in xenon sI hydrate and methane sI hydrate because both the large and small cages have high fractional occupancies in each of these sI hydrates and therefore there are few unit cells that contain unoccupied small cages.[1] Observation of a cage-dependent decomposition rate is expected because, assuming a first-order rate process, the decomposition rate depends on both the rate constant and the number of empty cages. However, more careful pressure-jump and temperature-jump sets of experiments similar to those described here may provide evidence regarding the distribution of unit cells model outlined in this work. Studies of these and other sI and sII gas hydrates would be beneficial for assessing the general applicability of the unit cell distribution model to the stability of nonstoichiometric compounds such as gas hydrates.

Conclusions

Thermally activated decomposition of C1−C2 sI hydrates has been monitored by using time-resolved ^{13}C MAS NMR spectroscopy as a function of guest composition and temperature. The C2 sI large cage is found to decompose more rapidly than the C1 sI small cage. A distribution of unit cells model, where unit cells contain zero, one, or two C1 molecules, is proposed based on the results of the decomposition experiments. Unit cells that contain zero C1 molecules are the least stable and decompose first, an implication of the distribution of unit cells model that is consistent with all the ^{13}C NMR data reported in this work.

Acknowledgment. Support for this work was provided by the National Science Foundation through research grant CTS01419204.

References and Notes

(1) Sloan, E. D., Jr. *Clathrate Hydrates of Natural Gases*, 2nd ed.; Marcel Dekker, Inc.: New York, 1998.

(2) Max, M. D., Ed. *Natural Gas Hydrate in Oceanic and Permafrost Environments*; Kluwer Academic Publishers: Boston, MA, 2000.

(3) Subramanian, S.; Kini, R. A.; Dec, S. F.; Sloan, E. D., Jr. *Chem. Eng. Sci*. **2000**, *55*, 1981.

(4) van der Waals, J. H.; Platteeuw, J. C. *Adv. Phys. Chem*. **1959**, *2*, 1.

(5) Koh, C. A.; Savidge, J. L.; Tang, C. C. *J. Phys. Chem*. **1996**, *100*, 6412.

(6) Henning, R. W.; Schultz, A. J.; Thieu, V.; Halpern, Y. *J. Phys. Chem. A* **2000**, *104*, 5066.

(7) Wang, X.; Schultz, A. J.; Halpern, Y. *J. Phys. Chem. A* **2002**, *106*, 7304.

(8) Staykova, D. K.; Kuhs, W. F.; Slamatin, A. N.; Hansen, T. *J. Phys. Chem. B* **2003**, *107*, 10299.

(9) Genov, G.; Kuhs, W. F.; Staykova, D. K.; Goreshnik, E.; Salamatin, A. N. *Am. Mineral*. **2004**, *89*, 1228.

(10) Koh, C. A.; Wisbey, R. P.; We, X.; Westacott, R. E.; Soper, A. K. *J. Chem. Phys*. **2000**, *113*, 6390.

(11) Thompson, H.; Soper, A. K.; Buchanan, P.; Aldiwan, N.; Creek, J. L.; Koh, C. A. *J. Chem. Phys.* **2006**, *124*, 164508.

(12) Pietrass, T.; Gaede, H. C.; Bifone, A.; Pines, A.; Ripmeester, J. A. *J. Am. Chem. Soc*. **1995**, *117*, 7520.

(13) Moudrakovski, I. L.; Sanchez, A. A.; Ratcliffe, C. I.; Ripmeester, J. A. *J. Phys. Chem. B* **2001**, *105*, 12338.

(14) Subramanian, S.; Sloan, E. D., Jr. *Fluid Phase Equil*. **1999**, *158*−*160*, 813.

(15) Kini, R. A.; Dec, S. F.; Sloan, E. D., Jr. *J. Phys. Chem. A* **2004**, *108*, 9550.

(16) Gupta, A.; Dec. S. F.; Koh, C. A.; Sloan, E. D., Jr. *J. Phys. Chem. C* **2007**, *111*, 2341.

(17) Freeman, R.; Hill, H. *J. Chem. Phys.* **1971**, *54*, 3367.

(18) Fukushima, E.; Roeder, S. B. W. *Experimental Pulse NMR. A Nuts and Bolts Approach*; Addison-Wesley Publishing Co.: Reading, MA, 1981; p 169.

(19) Dec. S. F.; Bowler, K. E.; Stadterman, L. L.; Koh, C. A.; Sloan, E. D., Jr. *J. Am. Chem. Soc.* **2006**, *128*, 414.

(20) Davidson, D. W.; Garg, S. K.; Grough, S. R.; Handa, Y. P.; Ratcliffe, C. I.; Ripmeester, J. A.; Tse, J. S.; Lawson, W. F. *Geochem. Cosmochim. Acta* **1986**, *50*, 619.

(21) Dharmawardhana, P. B.; Parrish, W. R.; Sloan, E. D., Jr. *Ind. Eng. Chem. Fundam*. **1980**, *19*, 410.